J Geod (2015) 89:313–329
DOI 10.1007/s00190-014-0777-x

ORIGINAL ARTICLE

Three-Corner Hat for the assessment of the uncertainty of non-linear residuals of space-geodetic time series in the context of terrestrial reference frame analysis

C. Abbondanza · Z. Altamimi · T. M. Chin · R. S. Gross · M. B. Heflin · J. W. Parker · X. Wu

Received: 23 June 2014 / Accepted: 30 October 2014 / Published online: 18 November 2014

Abstract We discuss the application of the Three-Corner Hat (TCH) to time series of space-geodetic station position residuals with the purpose of characterizing the uncertainties of GPS, VLBI, SLR, DORIS for the International Terrestrial Reference Frame (ITRF) determination. Adopting simulations, we show that, in the absence of time-correlated errors, TCH is able to fully recover the nominal uncertainties of groups of observations whose intrinsic precisions are remarkably dissimilar to one another, as is the case for the space-geodetic techniques. When time-correlated errors are predominant, as it happens with GPS, TCH is affected by the increased variance of the observations and its estimates are positively biased. TCH applied to 16 ITRF co-located sites confirms that GPS, albeit affected by time-correlated errors, is the most precise of the space-geodetic techniques. GPS median uncertainties are 1.1, 1.2 and 2.8 mm, for the north, east and height component, respectively. VLBI performs particularly well in the horizontal component, the median uncertainties being ≈2 mm. The height component is ∼3 times larger than the GPS one. SLR and DORIS median uncertainties exceed by far the 7 mm level on all of the three components. Comparing TCH results with station position repeatabilities, we find that the two metrics are in striking agreement for VLBI and DORIS, but not for SLR and GPS. The inconsistencies between TCH and station repeatabilities for co-located GPS and SLR point to the presence of either specific station-dependent biases or low-quality co-locations. Scaling factors derived adopting the ratio between TCH and median formal errors on the positions suggest the station position covariances have to be up-scaled for VLBI, SLR, DORIS and down-scaled for GPS.

Keywords Three-Corner Hat · GPS · VLBI · SLR · DORIS · International Terrestrial Reference Frame · Space-geodetic co-locations · Time-correlated noise

1 Introduction

The International Terrestrial Reference Frame (ITRF) is a linear reference frame relying on the combination of global position system (GPS), very long baseline interferometry (VLBI), satellite laser ranging (SLR) and doppler orbitography radiopositioning integrated on satellite (DORIS) observations. The most recent ITRF realizations, the ITRF2005 (Altamimi et al. 2007) and the ITRF2008 (Altamimi et al. 2011), stem from a two-step procedure in which (i) time series of station positions and Earth Orientation Parameters (EOPs) of space-geodetic (SG) techniques are individually stacked in order to estimate single-technique long-term reference frames and (ii) these latter, suitably weighted through their covariance matrices, are combined along with local ties.

Formal errors as reported in the covariance matrices of SG solutions do not generally reflect the existence of technique-dependent biases and are known to be overly optimistic. As a result, covariances of long-term reference frames are routinely scaled prior to any combination process so as to obtain a more realistic description of the SG uncertainties.

Electronic supplementary material The online version of this article (doi:10.1007/s00190-014-0777-x) contains supplementary material, which is available to authorized users.

C. Abbondanza (✉) · T. M. Chin · R. S. Gross · M. B. Heflin · J. W. Parker · X. Wu
Jet Propulsion Laboratory-California Institute of Technology, 4800 Oak Grove Drive, Pasadena, CA 91109, USA
e-mail: claudio.abbondanza@jpl.nasa.gov

Z. Altamimi
Laboratoire de Recherches en Géodésie, Institut National de l'Information Géographique et Forestière, Université Paris Diderot, Paris, France

The a posteriori variance factors (AVFs) obtained by stacking single-technique SG solutions are generally adopted in order to scale the covariance matrices. Root mean square (RMS) and weighted RMS (WRMS or repeatabilities) are also commonly adopted for characterizing the intrinsic precision of SG techniques. Yet AVFs, RMS and WRMS as determined in SG data reductions rely on post-fit residuals with respect to a linear frame and are therefore unavoidably affected by the presence of non-linear signals the current ITRF realizations do not account for.

The Three-Corner Hat (TCH) method can offer an alternative approach to quantifying the uncertainty of the SG techniques. Based on a difference approach leading to the removal of common signals from the observations, TCH is able to supply uncertainties which purely reflect the technique measurement errors. Originally conceived in metrology as a tool aimed at assessing the relative precision of oscillators and timing devices (Allan 1987), in the last decade TCH has been extended to a variety of SG applications.

Gambis (2002) showed how TCH can be applied to characterize the uncertainties in EOP observations, when measurements from three or more data sets are available. The Earth Orientation Centre of the International Earth Rotation and Reference Systems Service (IERS) has been routinely using TCH to scale the covariance matrices of EOPs prior to their combination (see, e.g. Gambis 2004; Bizouard and Gambis 2011).

Chin et al. (2005) adopted the approach to determine the uncertainty of multiple sets of GPS, VLBI and SLR-derived EOPs and discussed the application of a *generalized* TCH method allowing the data sets to have a certain degree of statistical correlation. Koot et al. (2006) characterized the internal noise of atmospheric angular momentum time series using a *generalized* TCH and discussed the impact of statistical correlations among the data sets analyzed.

Analysing station position residuals of the SG techniques determined for the ITRF2005 computation, Feissel-Vernier et al. (2007) quantified the noise content of GPS, VLBI, SLR and DORIS time series with the Allan variance (see, e.g. Allan 1987; Le Bail 2006) and attempted an evaluation of the uncertainty of the 4 SG techniques by means of TCH.

To apply TCH to SG positioning is in principle straightforward: adopting time series of position residuals at ITRF co-location sites with at least 3 SG techniques, pair-wise differences between the positions can be formed. The uncertainties of each SG technique can be thus recovered from the pair-wise difference processes with simple algebraical considerations.

In this investigation, TCH is applied to non-linear residuals of station positions derived from the SG data set adopted for the estimation of ITRF2008. In Sect. 2, the application of the TCH method to SG positioning is discussed, with particular emphasis on those aspects which might degrade the effectiveness of the approach, i.e. the dissimilar precisions of the SG techniques, the presence of technique-dependent systematic effects which cannot be removed through the difference process. Section 3 describes the data sets utilized and delineates the steps requested for the application of TCH to SG observations. Noise simulations are utilized in Sect. 4 with the purpose of assessing the effect of dissimilar precisions of the SG techniques on the TCH estimates. Section 5 discusses the results of TCH applied to the ITRF co-location sites and compare TCH estimates with intrinsic metrics such as AVFs, WRMS and formal errors. Conclusions are drawn in Sect. 6.

2 TCH in the context of SG positioning

The TCH approach is described with particular emphasis to the case of SG positioning. The TCH additive model decomposing the observations into the sum of signal and measurement noise is illustrated and its pertinence to the SG context is discussed.

TCH is applicable whenever observations of the same physical process are acquired from at least three different instruments. The approach assumes the observations can be decomposed as:

$$y^j(t) = x(t) + \varepsilon^j(t), \tag{1}$$

where $y^j(t)$ denotes the measurement acquired at the epoch t by the jth instrument, x represents the physical signal and $\varepsilon(t)$ the measurement noise of the jth instrument.

Providing all the instruments detect the same signal $x(t)$, the pair-wise difference δ^{jk} of the observations acquired by the instruments j and k uniquely depends on the measurement noises:

$$\delta^{jk}(t) = \varepsilon^j(t) - \varepsilon^k(t) \tag{2}$$

Assuming the error processes are stochastically uncorrelated, the variance of $\delta^{jk}(t)$ reads as:

$$\mathbf{D}(\delta^{jk}) = \mathbf{D}(\varepsilon^j) + \mathbf{D}(\varepsilon^k), \tag{3}$$

where $\mathbf{D}(\delta^{jk})$ denotes the empirical variance relative to the difference process δ^{jk}, $\mathbf{D}(\varepsilon^j)$ and $\mathbf{D}(\varepsilon^k)$ represent the variances of the noise errors ε^j and ε^k, respectively. The computation of the difference process of Eq. (2) requires the observations be simultaneous.

If measurements are available from three instruments, a linear system of three equations of the kind (3) in the unknowns $\mathbf{D}(\varepsilon^i)$, $\mathbf{D}(\varepsilon^j)$, $\mathbf{D}(\varepsilon^k)$ can be solved. The unknowns define the uncertainties of the observing techniques and their square roots will be equivalently indicated hereafter as either TCH-derived sigmas or TCH determinations/estimates. When observations are acquired by 4 instruments, as is the case for the ITRF sites in which 4 SG

Table 1 SG data sets used in the analysis

TC	T	DS	SOL	TR	Source
IGS	P	1997–2009	VC-MCS	Weekly	Collilieux et al. (2011)
IVS	R	1980–2008	NES-FNS	Session wise (daily)	Böckmann et al. (2010)
ILRS	L	1983–2008	VC-LCS	Weekly	Pavlis et al. (2011)
IDS	D	1993–2008	VC-MCS	Weekly	Valette et al. (2010)

TC in the first column identifies the technique center, T designates the SG techniques (P GPS, R VLBI, L SLR, D DORIS), DS is the time span of data, SOL identifies the kind of solution and the nature of its constraints (*NES-FNS* normal equations-free network solution, *VC-LCS* variance–covariance-loosely constrained solution, *VC-MCS* variance–covariance-minimally constrained solution), TR is the temporal resolution, the field source provides the reference for each submission

techniques are co-located, a redundant linear system can be solved in a least-squares fashion (Chin et al. 2005).

The additive model of Eq. (1) is particularly apt to describe the motion of SG stations. A number of studies that focussed on SG positioning (see, e.g. Collilieux et al. 2007; Ray et al. 2008; Davis et al. 2012) have consistently shown that station position time series stemming from the analysis of global networks can be decomposed as:

$$y(t) = d(t) + \eta(t) + \beta(t) + \varepsilon(t), \tag{4}$$

where the drift $d(t)$ identifies the linear component of the motion, $\eta(t)$ accounts for non-linear geophysical effects, $\beta(t)$ describes known technique-dependent systematic errors (e.g. draconitic signatures in GPS and DORIS systems) and $\varepsilon(t)$ represents the SG technique-related measurement noise.

When applying TCH to station position detrended residuals, the signal $x(t)$ in Eq. (1) uniquely reflects the non-linear geophysical motion of the site, i.e. $\eta(t)$. Assuming the co-located SG techniques consistently detect the same geophysical displacement, through the Eq. (2) the common-mode signal is canceled out in such a way that the difference process is purely representative of technique-dependent errors.

Whether or not simultaneously observing SG techniques at co-located sites are capable of sensing coherent geophysical signals is a subject of research investigated by Collilieux et al. (2007). Adopting an approach based on Kalman filtering, the authors showed that co-located GPS and VLBI time series are well correlated for every site with sufficient data. Also, the authors proved GPS height signals are spatially correlated over some continental regions and match VLBI and SLR annual signals in areas like South Africa and Australia. These findings corroborate the conclusion that the SG techniques are able to sense geophysically based displacements, thus enabling the application of the TCH method to SG positioning.

When applying TCH to SG observations, caution is nonetheless to be exercised. In fact recent studies such as Amiri-Simkooei et al. (2007), Ray et al. (2008, 2013) have proven GPS residual positions are affected by draconitic signatures. These introduce technique-specific sources of errors the difference process of Eq. (2) is not able to cancel out. Since we aim to provide TCH estimates free from known systematic effects, draconitic signatures will be removed from the SG observations.

Furthermore, as will be shown in Sect. 3.1, the 4 SG techniques are characterized by dissimilar precisions to one another and by noise processes which are not strictly stationary. The impact of groups of observations characterized by highly dissimilar precisions on TCH estimates will be assessed through simulations (cf. Sect. 4). Stochastic processes representative of the noise characteristics of the SG techniques will be used with the aim of verifying whether or not TCH is able to recover the nominal uncertainties of the simulated observations. Since the noise content of GPS global networks has proven to be affected by low-frequency flicker noise (see, e.g. Ray et al. 2008; Santamaría-Gómez et al. 2011), our simulations will account for the presence of time-correlated errors.

3 Space geodetic data sets and data reduction

The SG solutions utilized in this study are briefly described and the data reduction process leading to the application of the TCH approach is fully outlined in Sect. 3.1.

The official submissions released by the International VLBI Service for Geodesy and Astrometry (IVS), the International Laser Ranging Service (ILRS), the International GNSS Service (IGS) and the International DORIS Service (IDS) for the ITRF2008 computation have been adopted in this investigation. Solution (Software/technique) INdependent EXchange Format (SINEX)[1] files of weekly GPS, SLR and DORIS and daily VLBI sessions have been reduced in order to extract time series of residual station positions (cf. Table 1).

[1] http://www.iers.org/IERS/EN/Organization/AnalysisCoordinator/SinexFormat/sinex__cont.html.

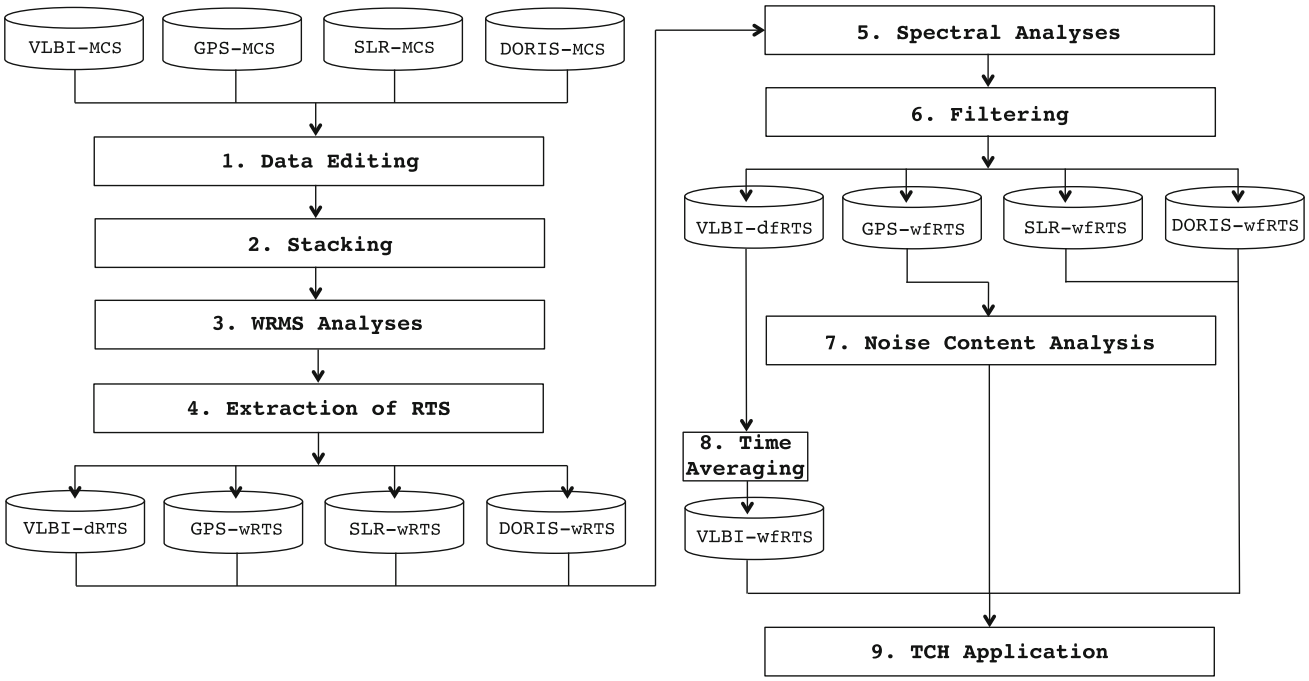

Fig. 1 Steps required for the TCH application to GPS, VLBI, SLR and DORIS. *Rectangles* identify the procedures which the data sets are subjected to. *Cylinders* represent SG data sets. The extension `MCS` qualifies the minimally constrained solutions. The extension `dRTS` (`wRTS`) identifies the daily (weekly) residual time series extracted at the ITRF sites and obtained as a result of the step `2`. The extension `dfRTS` (`wfRTS`) indicates the daily (weekly) filtered residual time series obtained as a result of the phase of filtering (step `6`)

3.1 Data reduction

The flow-chart of Fig. 1 delineates the steps required for the application of TCH to SG data sets. For an optimal usage of the covariance information of SG solutions, it is advisable to adopt input frames defined by means of minimal constraints. If loosely constrained or free network solutions are provided, as is the case for SLR and VLBI, minimal constraints should be applied in such a way that the covariances reflect the internal noise of the observations.

Following the procedures outlined in Altamimi et al. (2007), VLBI normal equations have been inverted applying minimal constraints over rotations and translations, whereas the covariance matrices of loosely constrained SLR solutions have been algebraically projected over rotations. The covariance matrices of the SLR solutions reflect not only the internal noise of the observations (i.e. the measurement noise). They also account for the portion of spatially correlated errors due to the presence of undefined frame parameters (i.e. the frame noise). To remove frame uncertainties from the covariance matrix of the SLR solutions, each of the SLR covariance matrices has been treated adopting the orthogonal covariance decomposition (i.e. projection) outlined by Sillard and Boucher (2001) (cf. Equations 19, 20 and 21 of the paper). Since frame origin and scale are intrinsically defined in SLR solutions, the SLR covariance matrices have been uniquely projected over rotations.

During the data editing (cf. step 1 in the flow-chart of Fig. 1), the minimally constrained SINEX files have been stacked individually for each technique with CATREF software (Altamimi et al. 2007). Minimal constraints with respect to ITRF2008 have been adopted to define the long-term reference frames derived from the stacking. Station position outliers with respect to the long-term frames have been identified and removed from the SG solutions.

The edited SINEX files have been re-stacked (cf. step 2) as follows: three rotations and three translations have been estimated for each SINEX file. No scale factor has been determined during the stacking in order to prevent the parameter from absorbing part of the non-linear station motion (see, e.g. Tregoning and van Dam 2005; Collilieux et al. 2009, 2012). However, to estimate the scale in this particular application should in principle lead to the same TCH results, since the difference process of Eq. (2) is aimed at removing common non-linear motions. Minimal constraints with respect to ITRF2008 have been applied to the long-term reference frames obtained as a result of the stacks. Station position residuals with respect to the long-term reference frames are inter-comparable and can be utilized when forming difference processes for the TCH application.

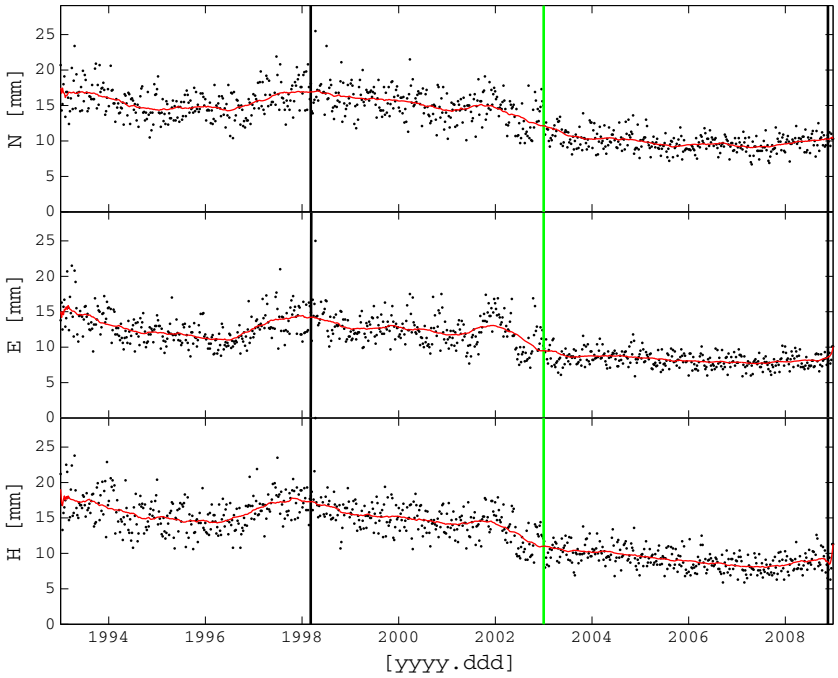

Fig. 2 WRMS (*black dots*) of the weekly DORIS SINEX files as a function of time. *The plots from top to bottom* refer to the north, east and height component, respectively. The abscissae report the epochs expressed in decimal year. The ordinates show the WRMS expressed in mm. *The red solid curve* is obtained applying a moving average filter with full width of 53 weekly WRMS determinations. *The black solid vertical lines*, corresponding to the time epochs 1998.18 and 2008.88, identify the time window in which common observations among the 4 SG techniques are available. The *green solid vertical line* identifies the epoch 2003.0 after which the technique performances remarkably improve

In step 3, the WRMS time series for the 4 SG techniques have been determined as detailed in Altamimi et al. (2002). The variation of WRMS provides an indication of the quality of the positioning as a function of time. WRMS have been computed adopting the residuals derived from the stacking and therefore reflect the presence of non-linear signals embedded in the station positions. TCH will be applied to time series included in the time window (1998.180, 2008.88) in which common observations among the 4 SG techniques can be found.

Figure 2 reports the temporal variation of DORIS WRMS. The vertical green line marks the time epoch 2003.0 and identifies 2 time segments ts_1 and ts_2, before and after 2003.0, respectively. The WRMS after 2003.0 clearly show an improvement which is attributable, as remarked by Altamimi et al. (2011), to the increased number of satellites (from 4 to 5) in the DORIS constellation. No significant improvement comparable to that of DORIS is detectable over the time window (1998.18, 2008.88) for the WRMS time series of GPS, VLBI and SLR, whose diagrams are accessible through the supplementary material. To account for the temporal variability of DORIS intrinsic precisions, it is therefore advisable to apply the TCH separately to the two time segments ts_1 and ts_2. As a result, whenever DORIS observations are present at ITRF co-locations, 2 TCH determinations for ts_1 and ts_2 will be provided.

Table 2 reports the median values of the WRMS for the 4 SG techniques computed over the two time segments. The median WRMS show the intrinsic precisions of the 4 SG techniques are considerably dissimilar, with GPS being the most precise technique followed by VLBI, SLR and DORIS. It is worth observing DORIS WRMS can be ∼10 times as large as GPS (cf. north component in ts_1). Also, an improvement of ∼5 mm in the median WRMS can be observed when passing from ts_1 to ts_2. TCH has not been specifically designed for dealing with groups of observations whose intrinsic precisions are highly dissimilar. The effect of the dissimilar performances of the 4 SG techniques on TCH will be investigated by means of simulations of noise processes in Sect. 4.

Table 2 Median values in mm of the WRMS for the north, east and height components of the 4 SG techniques

T	ts	North	East	Height
P	1	1.6	1.6	4.4
	2	1.3	1.4	4.0
R	1	2.6	2.7	7.1
	2	2.6	2.8	7.8
L	1	8.0	8.9	7.0
	2	7.4	8.4	6.0
D	1	15.1	12.3	14.8
	2	9.8	8.2	9.1

T in the first row indicates the SG technique (P GPS, R VLBI, L SLR, D DORIS), ts denotes the time segment over which the WRMS were computed: ts_1 refers to the time window [1998.18,2003.00], whereas ts_2 to [2003.00,2008.88]

During step 4, we extract time series of residual station positions for each SG technique at the ITRF sites. Linear trends as well as jumps affecting the station positions have been estimated during the stacking and removed when computing the residuals, utilizing the station position discontinu-

ities[2] defined for the ITRF2008. The adoption of detrended station position residuals ensures that dissimilarities in the velocities of co-located SG instruments at ITRF sites do not perturb the TCH estimates.

Spectral analyses applied to station position residuals (cf. step 5) have substantially confirmed what was found by Ray et al. (2008) for the residual station positions of ITRF2005: GPS stacked periodograms of station residuals are affected by periodic signatures which can be related to the fundamental GPS draconitic frequency of 1.04 cpy and are characterized by low-frequency flicker noise. Figure 3 visualizes the GPS stacked periodograms of the detrended and deseasonalized residual station positions where the fundamental draconitic frequency along with its overtones are marked in red. The dashed black line represents a power spectral density function monotonically decreasing as f^{-1} (f, frequency) and therefore consistent with a flicker noise spectrum. As can be observed by inspecting Fig. 3, the dashed black line fits the GPS periodograms rather well at the lowest frequencies. At higher frequencies, where the contribution of white noise and its integrals is stronger, the periodograms tend to flatten out. In addition, the GPS spectra appear not to be compatible with a power spectral density function decreasing as f^{-2}, representative of the spectrum of a random walk process. None of the GPS draconitic frequencies appears in the periodograms of the other SG techniques, whose background noise is mostly white (VLBI and SLR periodograms are reported in the supplementary material).

As shown in Fig. 4, DORIS stacked periodograms manifest sharp peaks corresponding to 3.09 and 6.18 cpy and are suggestive of a predominantly white background noise, particularly at higher frequencies. Similar to GPS, the anomalous spectral lines do not relate to any geophysical motions and are most likely to reflect systematic effects inherent to DORIS. The 3.09 cpy spectral line corresponds to ~118 days, i.e. the draconitic period for the satellite TOPEX. As pointed out by Gobinddass et al. (2009), geocenter-related parameters for DORIS exhibit distinct spectral features at the TOPEX draconitic frequencies. It is thus plausible to assume the periodograms of DORIS residual positions reflect the same generating mechanism.

As remarked in Sect. 2, we aim to provide TCH estimates free from known sources of systematic errors. Draconitic signatures affecting the SG techniques will be therefore removed (cf. step 6, filtering). Draconitic signals in GPS residual positions manifest themselves as broad-banded peaks in the spectral domain. Also, they do not exactly occur at multiples of the fundamental generating tone 1.04 cpy (Santamaría-Gómez et al. 2011). We therefore suggest their removal be executed by defining a suitable spectral band centered about the 1.04 cpy frequency and its overtones. Spectral bands with increasing semi-width of 0.10, 0.14 and 0.20 cpy have been considered. All of the frequencies included in such spectral bands have been least-squares fitted and filtered out from the GPS residuals and the spectra relative to the 3 spectral bands have been compared. We found the adoption of a semi-band-width of 0.14 cpy is adequate to remove the broad-band draconitic signatures. As for DORIS, the filtering based on the least-squares fits of the 3.09 cpy fundamental frequency and its overtones has proven apt to remove the draconitic signatures.

Prior to applying TCH, the seasonal components (i.e. the annual and semi-annual harmonics) have been least-squares fitted and removed from the residual positions of the 4 SG techniques. In the following, the term *filtered* is meant to indicate time series of residual positions wherein the linear trends, the seasonal components, the GPS and DORIS draconitic signatures have been removed.

During step 7, the noise content of GPS filtered time series has been quantified. The characterization of errors affecting GPS station position time series has long been dealt with in a variety of studies (see, e.g. Zhang et al. 1997; Mao et al. 1999; Williams et al. 2004). Most recently, applying spectral and maximum-likelihood estimator-based methods to homogeneously reprocessed GPS data derived from global networks, Santamaría-Gómez et al. (2011) have proven the combination of flicker and white noise to be the most appropriate description of GPS noise. The authors also concluded that physical random walk motion of the GPS monuments as detected in short baseline studies (see, e.g. Wyatt 1982, 1989; Langbein and Johnson 1997; Beavan 2005) cannot be identified in global GPS networks due to other sources of error being more conspicuous. Since our GPS solutions result from the reprocessing of global networks, it is legitimate to assume that the GPS noise $\varepsilon(t)$ follows an additive model:

$$\varepsilon(t) = a\omega(t) + b\varphi(t) \tag{5}$$

wherein ω identifies a Gaussian process with zero-mean and unitary variance (i.e. white noise), a is the amplitude associated with the Gaussian process, φ a flicker noise realization with unitary variance, b is its amplitude and t is time.

The noise content of each GPS filtered time series has been here quantified utilizing CATS software (Williams 2008). The software provides maximum-likelihood estimates of the noise amplitudes adopting an additive stochastic model which, in our case, is chosen to be:

$$\mathbf{C}_y = a^2\mathbf{I}_\omega + b^2\mathbf{J}_\varphi \tag{6}$$

where $\mathbf{C}_y$ identifies the covariance matrix of the filtered time series, the variance factors a^2 and b^2 define the square of the amplitude of white and flicker noise, respectively, $\mathbf{I}_\omega$ is the white noise identity matrix and $\mathbf{J}_\varphi$ the flicker noise covariance matrix. As detailed in Williams (2003), the matrix $\mathbf{J}_\varphi$, obtained through the fractional differencing approach (Hosk-

[2] Available at http://itrf.ensg.ign.fr/ITRF_solutions/2008/computation_strategy.php?page=2.

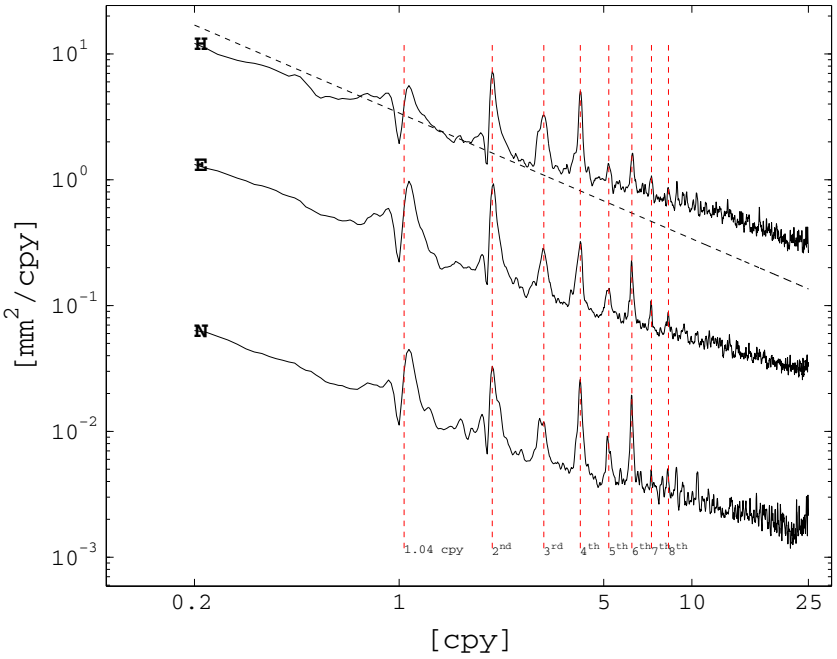

Fig. 3 Stacked Lomb–Scargle periodograms of detrended and de-seasonalized GPS time series with more than 100 observations in the log–log domain. Abscissae report the frequencies expressed in cpy, whereas the ordinates report the spectral density in mm^2/cpy. The *black solid curve on top of the graph* denoted with H displays the spectrum for the height component. Those denoted with E and N show the spectrum for the east and north component, respectively. For clarity of representation, the spectrum of the east and north component has been scaled by the quantities $10^{-1.0}$ and $10^{-2.3}$, respectively. *The dashed black line* shows the spectrum of a flicker noise. *Vertical dashed red lines* indicate draconitic frequencies for GPS from the fundamental generating tone at 1.04 cpy up to the 8th harmonic (i.e. the 7th overtone)

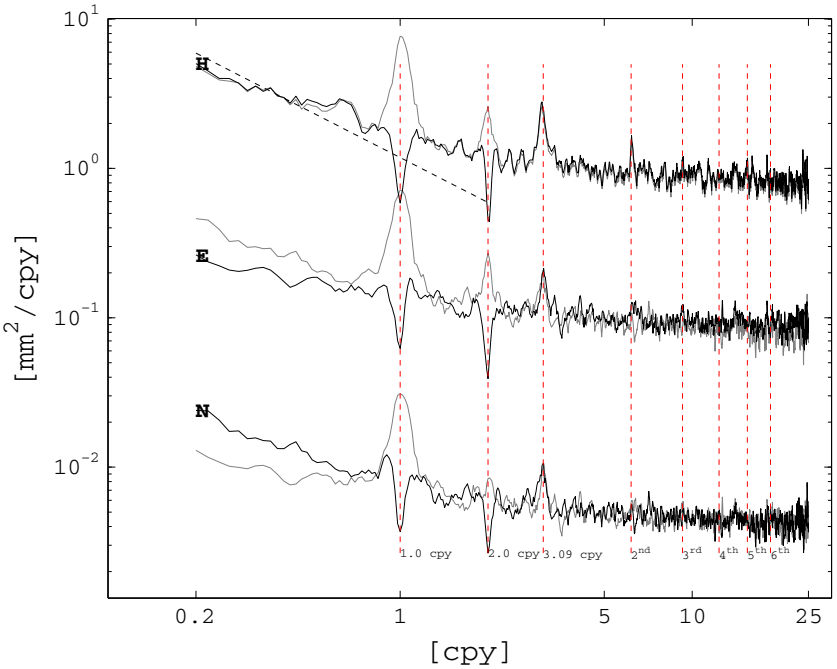

Fig. 4 Stacked Lomb–Scargle periodograms of DORIS time series with more than 100 observations in the log–log domain. Abscissae report the frequencies expressed in cpy, whereas the ordinates report the spectral density in mm^2/cpy. *The light gray solid curves* show the spectrum of the detrended residual time series whereas those in *black* display the spectrum of the detrended and de-seasonalized residual time series. *The dashed black lines* show the spectrum of a flicker noise. For clarity of representation, the spectrum of the east and north component has been scaled by the quantities $10^{-1.0}$ and $10^{-2.3}$, respectively. *The vertical dashed red lines* represent the annual (1.0 cpy) and the semi-annual (2.0 cpy) frequency and the draconitic frequencies for DORIS from the fundamental generating tone at 3.09 cpy up to the 5th overtone

Table 3 Noise content analyses of *filtered* GPS time series

	North			East			Height		
	a	*b*	*r*	*a*	*b*	*r*	a	*b*	*r*
Median	0.9	1.4	1.6	0.6	1.4	2.1	1.3	4.5	3.1
SD	1.3	1.5	1.5	1.1	2.1	1.8	2.0	4.0	3.0

The additive-noise model described in Eq. (5) has been adopted. The row *median* (*SD*) reports the median values (standard deviations) of a, b and r for all of the three components. Values of a are assigned in mm, b in mm/$y^{0.25}$ whereas units of r are $y^{-0.25}$

ing 1981), is scaled by the factor $\Delta T^{1/2}$, where ΔT is the sampling interval of the time series (weekly in our case). Since the diagonal elements of $\mathbf{C}_y$ are expressed in mm^2, $\mathbf{I}_\omega$ is dimensionless and the element of $\mathbf{J}_\varphi$ are expressed in $y^{0.5}$, in order to make Eq. (6) dimensionally homogeneous, the units of a are mm, those of b are mm/$y^{0.25}$, whereas the ratio $r = \frac{b}{a}$ is expressed in $y^{-0.25}$. For ease of representation, units of the ratio r will be omitted hereafter.

White and flicker noise amplitudes of GPS filtered time series with more than 100 observations have been estimated and statistics related to these determinations are reported in Table 3. The percentages of stations with $r > 1$ are 74, 83 and 96 % for the north, east and height components, respectively. Most of the GPS stations are therefore characterized by a content of flicker noise larger than the white, with slightly dissimilar behaviour for the three components. The height component turns out to be the most affected in terms of time-correlated errors, the median flicker noise amplitude being three times larger than the horizontal ones.

Prior to applying TCH, daily (filtered) time series of VLBI residual positions have been aggregated into weekly averages (cf. step 8 in the flow-chart of Fig. 1). For each VLBI station, the daily residual positions have been grouped into weekly bins matching the GPS weeks. When more than one residual position is included into the weekly bins, the daily observations are averaged into weekly positions. The averaged weekly positions are then linearly interpolated in time so as to match the central epoch of the GPS week.

4 Simulations

Simulations of noise processes are utilized in order to quantify the extent at which dissimilar precisions of the SG techniques and time-correlated errors can impact the TCH results. When examining the stacked periodograms of the residual station positions in Sect. 3.1, no substantive evidence of random walk has been found in any of the SG techniques. Therefore, our simulations uniquely account for the presence of white and flicker noise.

Time-correlated errors have been widely investigated in a large number of geodetic studies focussing on the impact of the noise structure in GPS velocity uncertainty estimates and different approaches to noise simulations have been proposed (see, e.g. Zhang et al. 1997; Mao et al. 1999; Williams 2003).

In this study, following Kasdin (1995), flicker noise is simulated adopting an autoregressive formulation:

$$\begin{aligned}\varphi_n = &-\ell_1\varphi_{n-1} - \ell_2\varphi_{n-2} \\ &-\ell_3\varphi_{n-3} - \cdots - \ell_j\varphi_{n-j} + \cdots + w_n\end{aligned} \tag{7}$$

where n denotes the time index, j represents the autoregressive order (i.e. the number of the ℓ_j coefficients), φ_n and w_n are realizations of flicker and white noise, respectively, at the nth time epoch. The kth autoregressive coefficient ℓ_k can be recursively defined as:

$$\begin{aligned}\ell_0 &= 1 \\ \ell_k &= \left(k - \frac{3}{2}\right)\left(\frac{\ell_{k-1}}{k}\right)\end{aligned} \tag{8}$$

In our simulations, the autoregressive order j [cf. Eq. (7)] is chosen to be equal to the number of simulated observations.

Three stochastic processes $\boldsymbol{\varepsilon_1}$, $\boldsymbol{\varepsilon_2}$, $\boldsymbol{\varepsilon_3}$, with noise characteristics chosen so as to mimic those of the SG time series, have been simulated and used as input to TCH. $\boldsymbol{\varepsilon_1}$ represents the GPS noise content and is therefore defined as the combination of white and flicker noise:

$$\varepsilon_1(t) = a_1\left[\omega(t) + r\varphi(t)\right]. \tag{9}$$

The parameters a_1 and r of Eq. (9) enable to control the amount of white (ω) and flicker (φ) noise injected into $\boldsymbol{\varepsilon_1}$. In our simulations, a_1 varies in the range (0.1, 6) mm whereas r in (0, 6), these values being representative of the median noise content of the GPS network analyzed in Sect. 3 (cf. Table 3). We observe that, for fixed values of the white noise content a_1, as the flicker noise amplitude increases, the variance of ε_1 increases.

$\boldsymbol{\varepsilon_2}$ and $\boldsymbol{\varepsilon_3}$, designed to mimic the noise characteristics of the least precise SG techniques (i.e. VLBI, SLR and DORIS), are white noise processes with amplitudes $a_2 = 4$ mm and $a_3 = 16$ mm, respectively. Time series with 520 elements have been generated, this value being representative of the maximum number of simultaneous observations for the ITRF co-locations adopted in this study. Throughout our simulations, a_2 and a_3 have been kept fixed while increasing the values of a_1 and r.

By setting a_1, r, a_2 and a_3 and generating white and flicker noises, a realization of the three noise processes ε_1, ε_2 and ε_3 can be simulated. TCH can be applied to the three noise processes, with the aim of verifying whether the algorithm is able to recover the nominal uncertainties a_1, a_2 and a_3 of the three time series. When applying TCH to the generic ith realization of noise processes, we can define the following quantity:

$$\delta_j^i(a_1, r) = \sigma_j^i - a_j, \tag{10}$$

where σ_j^i is the TCH estimate and a_j the white noise amplitude of the jth noise process ($j = 1, 2, 3$). δ_j^i isolates the contribution of time-correlated errors in the TCH estimates. For each value of a_1 and r, we simulated a number n_e of different realizations of noise processes. TCH has been individually applied to each of the n_e realizations. By averaging δ_j^i over the number of realizations n_e, the following statistic can be defined:

$$e_j\,(a_1, r) = \frac{1}{n_e}\sum_{i=1}^{n_e}\delta_j^i(a_1, r) \tag{11}$$

In our simulations, n_e, number of realizations, has been set to 50.

The average discrepancy of Eq. (11) has been determined for each of the three noise processes so as to quantify the impact of the increasing level of flicker noise on the TCH estimates. The curves plotted in Fig. 5 show the discrepancy e_1 for ε_1 as a function of the ratio r and parameterized for increasing values of the white noise amplitude a_1.

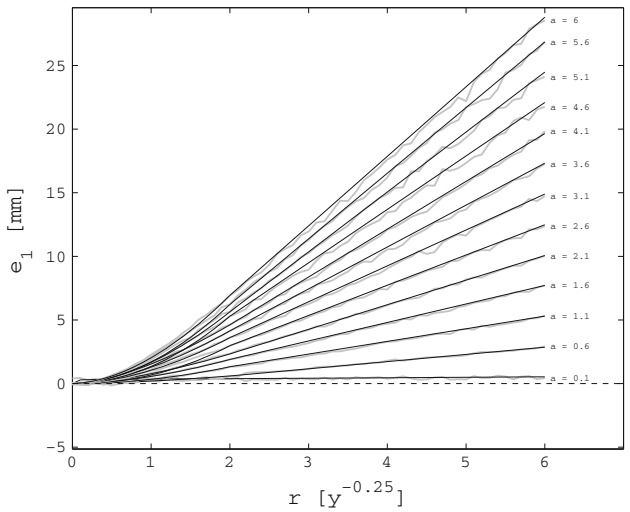

Fig. 5 Average discrepancy e_1 as described in Eq. (11) computed for the noise process ε_1 affected by time-correlated errors. e_1 is plotted as a function of the ratio r and parameterized according to increasing values of the background white noise amplitude a, expressed in mm. The ordinates report e_1 expressed in mm. In the abscissae the ratio r is reported

We observe that e_1 is a monotonically increasing function of r and a_1 always assuming positive values. As r tends to 0, all of the curves reported in Fig. 5 converge to zero regardless of the level of background white noise a_1. Therefore, in the absence of time-correlated noise, TCH is able to fully recover the nominal uncertainties of groups of observations, even when these are remarkably dissimilar to one another. When the time-correlated errors predominate over white noise ($r \gg 1$), TCH proves affected by the increased variance of the observations. The discrepancy increases as the content of flicker noise injected in the observations augments.

Unlike e_1, the discrepancies e_2 and e_3 are randomly distributed with zero-mean and dispersion about the mean less than 0.3 mm. These results confirm as expected the TCH estimates for ϵ_2 and ϵ_3 are not affected either by the presence of time-correlated errors in ϵ_1 or by the dissimilar nominal uncertainties of the noise processes. No significant differences of e_1 have been found when varying the white noise amplitudes a_2 and a_3. Therefore the discrepancy e_1 does not depend upon the white noise content of ϵ_2 and ϵ_3. The curves in Fig. 5 have been interpolated estimating the parameters (α, β, k, q) of the following function:

$$\varepsilon(a, r) = \begin{cases} \alpha r^{\beta} & \text{if } r \leq 2 \\ kr + q & \text{otherwise} \end{cases} \tag{12}$$

Table S1 reported in the supplementary material collects the parameters of the interpolating function of Eq. (12) for increasing values of the white noise amplitude a. By using such parameters, it is therefore possible to provide an indication of the contribution of time-correlated errors to the TCH-derived sigmas.

5 Results and discussion

Results of the TCH application to the ITRF co-located sites are illustrated. Simultaneous observations of the residual positions have been identified at ITRF co-locations having at least 3 observing techniques and co-located sites with less than 30 common observations have been discarded from the analyses. Out of all the ITRF co-locations, only 16 turned out to be characterized by a sufficient number of observations (cf. Table 4).

All of the 16 ITRF sites are co-located with GPS. Six sites host co-locations among GPS, SLR and DORIS. Three sites are co-located with GPS, VLBI and DORIS. Four are GPS, VLBI and SLR co-locations. Hartebeesthoek (South Africa) is the only 4-way co-location with a sufficient number of simultaneous observations. TCH has been individually applied to each site shown in Table 4 adopting time series of filtered residual positions (i.e. free from draconitic signatures, detrended and de-seasonalized) derived from the stacking outlined in Sect. 3.1. For all of the ITRF co-locations

Table 4 List of the ITRF co-locations TCH has been applied to

DOMES	ϕ	λ	Site name	P	R	L	D
10317	78.55	11.56	Ny-Ålesund (Norway)	NYA1	7331	–	SPIA/SPJB
10503	60.13	24.23	Metsahovi (Finland)	METS	–	7806	META/METB
12734	40.46	16.70	Matera (Italy)	MATE	7243	7939/7941	–
14201	48.95	12.88	Wettzell (Germany)	WTZR	7224	8834	–
21605	30.93	121.20	Shanghai (China)	SHAO	7227	7821/7837	–
30302	−25.53	27.42	Hartebeesthoek (South Africa)	HARB	7232	7501	HBKA/HBLA/HBKB/HBMB
40408	64.83	212.50	Fairbanks (USA)	FAIR	7225	–	FAIA/FAIB
40424	21.99	200.34	Kauai (USA)	KOKB	7298	–	KOKA/KOLB
40442	30.40	255.59	Fort Davis (USA)	MDO1	7613	7080	–
40451	38.83	283.17	Greenbelt (USA)	GODE	–	7105	GREB
40497	32.72	243.58	Monument Peak (USA)	MONP	–	7110	MONB/MOOB
41719	−36.66	286.97	Concepcion (Chile)	CONZ	7640	7405	–
42202	−16.36	288.51	Arequipa (Peru)	AREQ	–	7403	AREA/AREB/ARFB
50103	−35.22	148.98	Tidbinbilla (Australia)	TIDB	–	7843	ORRB
50119	−35.13	149.01	Mount Stromlo (Australia)	STR1	–	7825/7849	MSOB/MSPB
92201	−17.47	210.39	Papeete (Tahiti)	THTI	–	7124	PAPB/PAQB/PATB

Each site is identified by its DOMES number in column 1, followed by latitudes (ϕ) and longitudes (λ) in degrees in columns 2 and 3, respectively, and the site names in column 4. Columns P (GPS), R (VLBI), L (SLR) and D (DORIS) report the conventional station codes used in the SG data reductions. When more than one station code is present in columns L and D, residual time series have been merged prior to applying TCH

hosting DORIS stations, TCH has been applied separately to the two distinct time segments ts_1 and ts_2. At the sites in which DORIS is not present, TCH has been applied to the entire time span of the observations.

TCH results listed per site and per component along with WRMS and median formal errors have been reported in Table 5. For some of the co-located sites the number of simultaneous observations utilized for the application of TCH differs depending upon the component of the local frame (cf. column `n` of Table 5). In such cases, the TCH algorithm applied to the entire set of simultaneous observations fails to provide non-negative variances. Whenever this occurs, a subset of simultaneous observations is selected through an iterative procedure by removing a progressively increasing number of observations until the TCH algorithm provides non-negative variances. TCH and WRMS have been computed adopting the same sample of observations in such a way that the two metrics can be consistently compared. In GPS case, TCH results include the contribution of time-correlated errors, whose impact has been simulated in Sect. 4.

Figure 6 visualizes the TCH estimates at ITRF co-locations and helps compare and establish the degree of (relative) precision of the 4 SG techniques. It can be observed that, on the whole, the most precise technique is GPS for most of the sites. Table 6 collects the median values of TCH estimates. These statistics clearly confirm the hierarchy of the SG techniques with GPS being the most precise followed by VLBI, SLR and DORIS. Notwithstanding GPS is affected by sizeable time-correlated errors particularly on the height component, the technique proves the most precise.

GPS performs better in the horizontal than in the vertical component, the TCH median values of the north and east components being ∼3 times smaller than the height. Such a pattern is likewise reflected by the formal uncertainties of the GPS solutions. The plots of Fig. 6 spotlight anomalous GPS stations with TCH-derived sigmas larger than 5 mm in at least one of the three components. These are METS (10503, Metsahovi, Finland), AREQ (42202, Arequipa, Peru) and THTI (92201, Papeete, Tahiti). Also, Fort Davis (40442, USA) is the only site in which GPS is not the most precise technique (cf. height component, time segment ts_0 for 40442 in Fig. 6).

As pointed out by the ITRF2008 discrepancies between SG and terrestrial tie observations,[3] Metsahovi is characterized by anomalous residuals (larger than 1 cm) on the height component of the vector connecting the GPS (METS) and SLR (7806) stations. Such anomalies are confirmed by the TCH estimates and are suggestive of technique-dependent effects at the site.

Arequipa is highly seismic and we expect the site seismicity to degrade the quality of the SG positioning thus causing the TCH-derived sigmas for all of the SG techniques to drastically augment.

[3] The list of ITRF2008 discrepancies can be accessed at http://itrf.ensg.ign.fr/ITRF_solutions/2008/ITRF2008.php.

The TCH anomalies for THTI are attributable to the remarkably high level of time-correlated errors, as pointed out by the noise content analysis described in Sect. 3.1. Flicker noise amplitudes are 2.3, 3.2 and 10.7 mm/$y^{0.25}$ for the north, east and height component, respectively. The GPS stations at Greenbelt (GODE) and Tidbinbilla (TIDB) were equipped with uncalibrated radomes which are known to introduce biases in the height component. However TCH determinations for both of the stations are not suggestive of site anomalies.

VLBI stations perform particularly well in the horizontal components, with TCH median values of ≈2 mm. TCH results for the height component exhibit a larger scatter with median value of 6.2 mm (cf. Table 6).

SLR is characterized by TCH median uncertainties of 8.5 and 7.6 mm, for the north and east component, respectively. TCH on the height attains the value of 9 mm. As can be deduced by inspecting the SLR TCH results in Fig. 6, the SLR stations at Shanghai (21605) and Metsahovi (10503) turn out to be characterized by the worst performances, with TCH-derived sigmas up to 20.8 mm.

Table 5 TCH estimates for the ITRF co-locations listed in Table 4

DOMES	ts	T	North					East					Height				
			n	TCH	*W*	σ	*R*	*n*	TCH	*W*	σ	*R*	*n*	TCH	*W*	σ	*R*
10317	1	P	157	1.2	0.9	1.3	0.9	127	0.5	0.7	1.2	0.4	157	2.6	3.6	5.8	0.4
		R		1.9	1.9	0.7	2.5		1.8	1.7	0.6	2.9		5.7	7.5	1.8	3.2
		D		8.7	8.6	3.0	2.9		6.8	6.1	2.7	2.6		10.1	9.0	2.7	3.7
10317	2	P	196	1.1	0.5	1.1	1.0	196	0.9	1.0	1.0	0.9	196	2.8	3.2	4.9	0.6
		R		1.4	1.5	0.6	2.4		1.3	1.4	0.6	2.2		5.4	5.2	1.7	3.2
		D		6.0	6.0	1.8	3.3		5.1	4.7	1.7	3.1		7.1	6.9	1.6	4.3
10503	1	P	43	1.5	0.9	1.2	1.2	58	4.0	0.8	1.0	3.8	58	7.0	2.7	3.2	2.2
		L		19.7	12.0	8.6	2.3		20.8	11.6	8.0	2.6		18.1	11.6	3.8	4.7
		D		11.4	10.5	3.6	3.1		13.2	13.4	5.0	2.6		12.0	13.0	4.6	2.6
12734	0	P	235	1.9	0.7	1.1	1.7	235	1.4	0.8	1.1	1.3	235	3.9	2.4	3.6	1.1
		R		1.3	2.0	0.8	1.6		1.7	1.8	0.8	2.1		4.5	5.1	2.0	2.2
		L		9.6	7.6	5.6	1.7		11.1	8.5	5.3	2.1		10.8	6.7	2.2	4.9
14201	0	P	386	0.5	0.8	1.2	0.4	444	0.6	0.7	1.0	0.6	504	2.2	2.7	3.6	0.6
		R		1.7	1.5	1.1	1.6		1.5	1.4	1.0	1.5		3.4	3.6	2.2	1.6
		L		9.3	7.4	4.9	1.9		8.6	7.4	4.6	1.9		9.5	8.4	1.3	7.4
21605	0	P	56	1.3	1.5	1.7	0.8	39	1.7	0.9	1.8	0.9	51	1.5	2.8	7.5	0.2
		R		1.6	1.6	0.9	1.7		0.6	1.6	1.0	0.6		5.7	4.9	2.3	2.5
		L		11.4	10.6	6.9	1.6		13.1	11.0	6.6	2.0		19.5	15.6	3.5	5.5
30302	1	P	66	1.2	1.0	1.6	0.8	66	1.2	1.0	1.6	0.8	63	1.0	2.2	5.7	0.2
		R		3.0	3.3	1.6	1.9		2.0	2.5	1.4	1.4		7.7	7.9	4.2	1.8
		L		7.1	6.4	4.9	1.5		5.3	4.5	4.7	1.1		10.6	3.3	1.5	6.8
		D		10.3	9.6	3.3	3.2		14.1	13.2	6.5	2.2		5.2	10.2	4.6	1.1
30302	2	P	75	2.3	0.8	1.3	1.8	75	2.4	0.6	1.3	1.8	75	2.8	2.1	4.9	0.6
		R		4.5	3.6	1.3	3.4		4.8	3.0	1.5	3.3		6.4	5.9	3.1	2.0
		L		6.8	7.1	5.2	1.3		3.5	4.8	4.7	0.8		9.1	7.8	1.6	5.7
		D		6.3	6.1	2.3	2.8		12.2	12.1	4.6	2.7		8.9	8.7	3.2	2.8
40408	1	P	223	1.5	1.4	1.6	0.9	152	0.5	0.9	1.2	0.4	223	1.7	3.9	4.9	0.3
		R		1.3	1.6	0.9	1.4		2.0	1.8	0.9	2.2		6.2	4.5	2.2	2.8
		D		8.4	8.0	3.0	2.8		9.6	9.6	3.8	2.5		12.2	11.9	3.4	3.6
40408	2	P	133	0.6	0.9	1.4	0.4	83	0.6	0.8	1.0	0.6	133	3.6	3.4	4.3	0.8
		R		2.2	1.5	0.9	2.4		1.4	1.2	0.9	1.6		2.1	3.0	2.3	0.9
		D		8.2	6.8	4.3	1.9		7.1	6.8	5.1	1.4		8.9	7.6	5.0	1.8
40424	1	P	260	0.8	1.0	1.3	0.6	244	0.5	1.3	1.6	0.3	260	3.5	3.8	5.2	0.7
		R		3.7	3.7	1.3	2.9		4.2	3.9	1.2	3.4		7.7	6.9	2.5	3.0
		D		14.7	14.0	3.3	4.4		19.7	19.3	6.6	3.0		16.4	15.7	4.6	3.6

Table 5 continued

DOMES	ts	T	North					East					Height				
			n	TCH	*W*	σ	*R*	*n*	TCH	*W*	σ	*R*	*n*	TCH	*W*	σ	*R*
40424	2	P	278	1.1	0.8	1.0	1.1	165	0.7	0.9	1.1	0.7	278	2.5	2.6	3.6	0.7
		R		3.8	3.7	2.0	1.9		3.5	3.7	1.8	1.9		6.8	6.4	3.0	2.3
		D		7.9	7.9	2.2	3.7		9.4	9.3	4.1	2.3		8.7	8.7	3.1	2.8
40442	0	P	64	0.8	0.8	1.1	0.7	75	1.0	0.9	1.2	0.8	75	4.1	2.8	4.5	0.9
		R		0.3	0.3	0.3	1.0		0.6	1.1	0.3	1.9		1.0	4.3	0.8	1.2
		L		7.1	7.5	4.7	1.5		7.4	6.9	4.6	1.6		6.2	6.4	1.5	4.1
40451	1	P	117	0.8	1.4	1.2	0.7	98	0.8	0.9	1.2	0.7	114	1.0	3.1	4.1	0.2
		L		6.6	6.4	4.6	1.4		7.6	5.6	4.1	1.9		5.6	3.7	1.1	5.3
		D		11.0	10.6	3.4	3.2		13.1	13.2	6.3	2.1		11.0	10.4	4.6	2.4
40451	2	P	232	2.9	0.7	1.0	2.8	232	1.4	0.7	1.0	1.4	108	1.4	2.4	3.8	0.4
		L		8.5	6.1	5.3	1.6		9.3	5.8	4.9	1.9		8.1	3.3	1.7	4.8
		D		7.9	7.9	2.4	3.3		9.4	9.1	4.7	2.0		11.1	10.3	3.5	3.1
40497	2	P	85	0.6	0.6	1.4	0.4	131	4.5	0.7	1.3	3.4	131	1.0	1.9	5.0	0.2
		L		6.6	6.0	4.8	1.4		7.1	5.3	4.7	1.5		7.1	3.8	1.4	4.9
		D		4.8	4.9	2.1	2.3		8.5	9.2	4.2	2.0		6.4	6.3	3.1	2.1
41719	0	P	198	2.5	1.1	1.4	1.8	108	0.5	1.3	1.3	0.4	198	2.8	2.7	4.0	0.7
		R		3.7	4.0	2.3	1.6		3.0	3.4	1.8	1.6		9.0	9.0	7.1	1.3
		L		10.4	8.8	5.4	1.9		12.4	12.3	6.5	1.9		10.0	5.7	2.0	5.0
42202	1	P	123	3.6	1.1	1.5	2.3	123	5.2	1.5	1.7	3.0	123	6.6	2.6	5.6	1.2
		L		10.8	7.3	5.9	1.8		10.7	6.7	6.5	1.7		9.0	4.4	2.3	3.9
		D		14.7	13.2	5.0	2.9		19.7	18.9	10.5	1.9		19.1	18.3	7.0	2.7
50103	1	P	45	0.9	1.2	1.5	0.6	46	1.5	1.3	1.8	0.8	46	3.1	2.4	4.4	0.7
		L		9.3	6.3	5.1	1.8		5.9	6.2	5.0	1.2		7.2	5.8	1.6	4.6
		D		17.1	16.0	6.2	2.8		19.5	19.1	13.5	1.4		27.1	23.8	9.1	3.0
50119	1	P	120	0.7	0.8	1.8	0.4	168	3.1	1.0	1.8	1.7	168	2.5	3.1	6.2	0.4
		L		6.1	5.8	4.4	1.4		7.0	5.6	4.4	1.6		5.9	4.3	1.4	4.3
		D		11.3	11.2	3.8	3.0		15.3	14.3	6.9	2.2		16.2	14.5	5.1	3.2
50119	2	P	185	0.5	0.6	1.7	0.3	198	1.9	1.0	1.7	1.1	198	2.2	2.2	6.0	0.4
		L		5.6	4.4	4.1	1.3		6.6	5.4	4.0	1.6		5.4	3.6	0.9	6.1
		D		5.9	5.9	2.4	2.5		10.0	10.1	4.7	2.1		7.3	7.4	3.2	2.3
92201	1	P	74	3.5	1.4	1.4	2.4	73	8.2	1.2	1.8	4.5	73	7.7	3.3	5.9	1.3
		L		12.9	5.3	6.1	2.1		11.7	5.3	6.3	1.8		13.7	3.6	2.7	5.1
		D		12.1	11.7	4.5	2.7		18.8	18.2	8.7	2.2		11.9	12.8	6.5	1.8
92201	2	P	45	0.7	0.8	1.1	0.6	95	2.9	0.9	1.3	2.2	95	3.3	2.7	3.9	0.8
		L		9.0	6.9	7.9	1.1		12.5	6.8	8.2	1.5		13.9	4.9	4.5	3.1
		D		9.8	8.5	2.3	4.2		11.3	11.2	4.9	2.3		10.0	9.6	3.6	2.8

The first column reports the DOMES number, ts refers to the time segment in which the TCH has been applied (cf. Sect. 3.1). When ts = 0, TCH is applied to the entire time span of available observations. T is the SG technique (P GPS, R VLBI, L SLR, D DORIS), *n* the number of simultaneous observations adopted in the TCH analyses. TCH, *W* and σ collect TCH, WRMS and median formal errors, respectively, all expressed in mm. *R* reports the dimensionless ratio between TCH/σ

In almost all of the co-locations, DORIS is the least performing technique with TCH median values well above the 1 cm level on almost all of the three components (cf. Table 6). By looking at the DORIS TCH results plotted in Fig. 6, an overall improvement is detectable when passing from time segment ts_1 to ts_2. The TCH-derived sigmas therefore reproduce the improvement testified by the WRMS time series of Fig. 2. The worst DORIS performances relate to the station at Tidbinbilla. Tidbinbilla is in fact an anomalous co-location wherein the distance between the DORIS and the GPS station is considerably large (≈25 km). In our analysis, we made the assumption the large inter-technique separa-

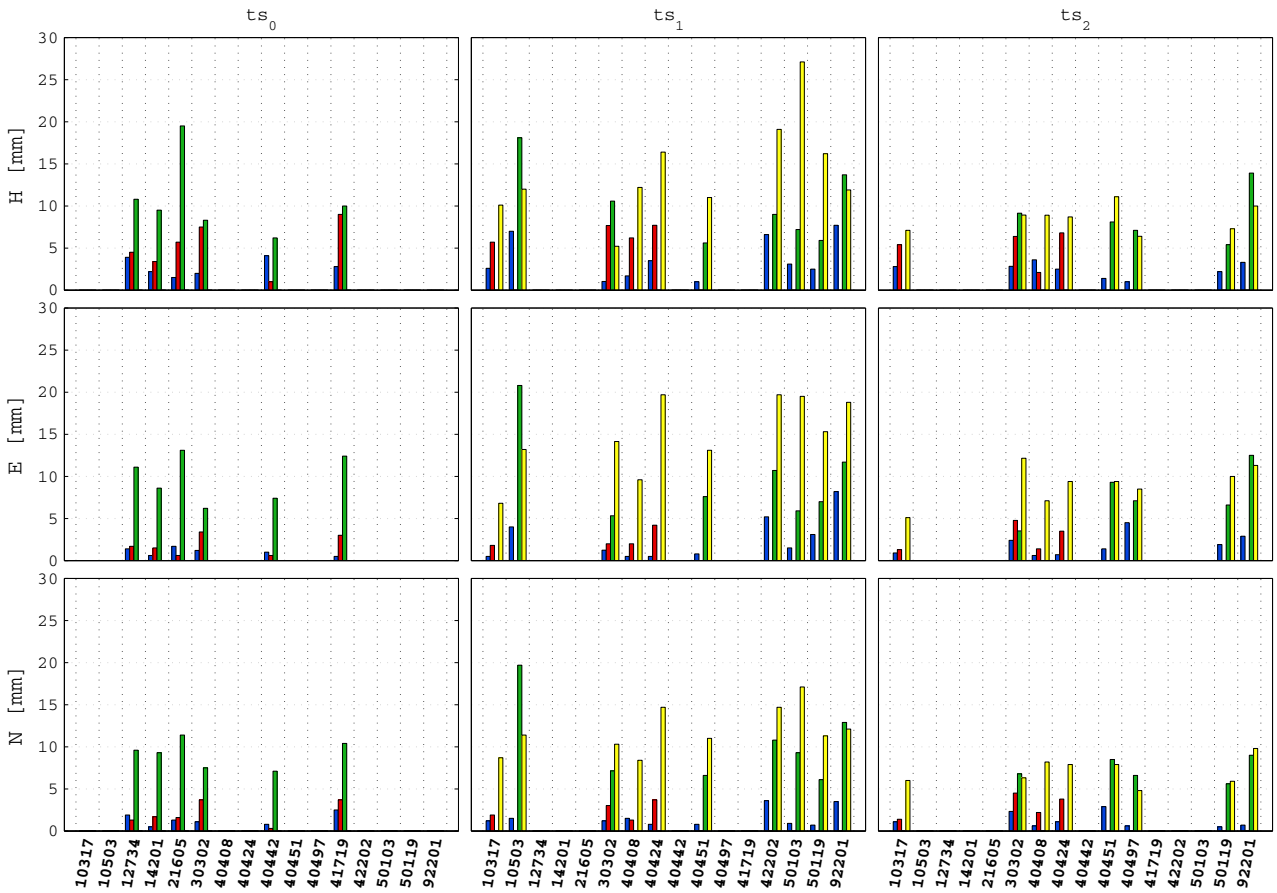

Fig. 6 *Bar plot* of the TCH estimates reported in Table 5. Results are plotted per components and per time segments and *color-coded* according to the SG technique. *Blue bars* represent GPS, *red bars* correspond to VLBI, *green bars* to SLR and those *yellow* to DORIS. In the abscissae, the DOMES numbers of the ITRF co-location sites are indicated. The ordinates report the TCH-derived sigmas expressed in mm

Table 6 Median values of the TCH estimates (column TCH in mm), of the ratios ρ = TCH/WRMS (column ρ) and R = TCH/σ (column R) computed over all the ITRF sites reported in Table 4

T	North			East			Height			s_0
	TCH	ρ	R	TCH	ρ	R	TCH	ρ	R	
P	1.1	1.2	0.8	1.2	0.9	0.8	2.8	0.8	0.6	0.9
R	2.2	1.0	1.9	2.0	1.1	2.1	6.2	1.0	2.0	5.5
L	8.5	1.3	1.5	7.6	1.2	1.6	9.0	1.6	4.9	4.4
D	9.2	1.0	3.0	11.7	1.0	2.2	10.6	1.0	2.8	3.2

Column T indicates the SG technique (P GPS, R VLBI, L SLR, D DORIS). The column s_0 reports the square root of the AVF obtained from the stacks of the SG techniques

tion does not affect the quality of the co-location. Yet the anomalous TCH estimates at Tidbinbilla suggest there may be uncommon motion patterns among the three co-located techniques thus making the site inapt for the TCH application.

The plots in Fig. 7 visualize the ratio ρ = TCH/WRMS for each SG technique at the co-locations of Table 4. Values of ρ larger than 1 are suggestive of technique-dependent systematic effects which do not show up either in the WRMS or in the median formal errors but are reflected in the TCH estimates.

As can be deduced by inspecting the median ratios ρ in Table 6, TCH and WRMS are in striking agreement for VLBI and DORIS, thus suggesting the WRMS can be used as a proxy for TCH at those sites wherein the application of the method is not feasible. As to SLR, the ratios ρ of the vertical component is more scattered than the horizontal, with values considerably larger than 2. Such anomalies might point once

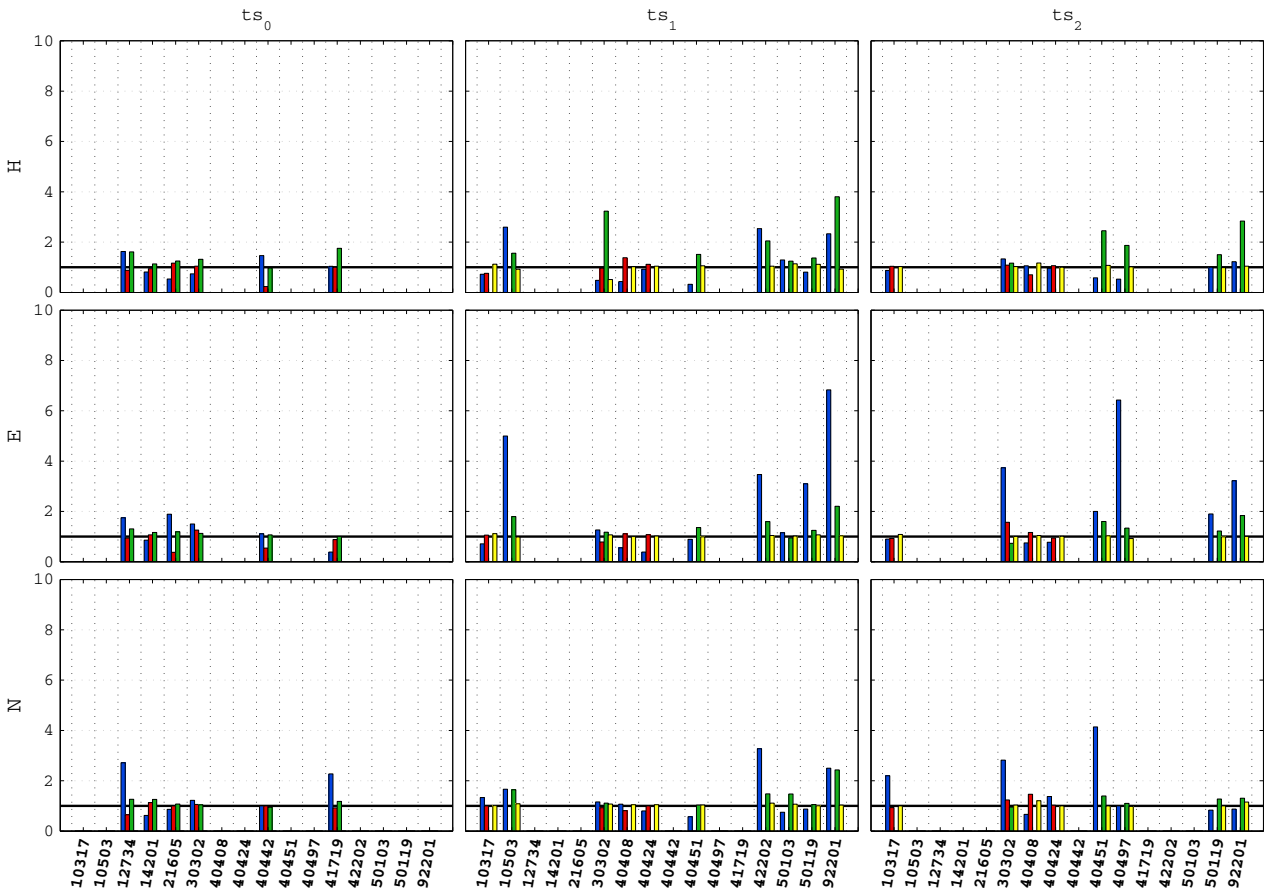

Fig. 7 *Bar plot* of the ratio ρ = TCH/WRMS between the TCH-derived sigmas and the repeatabilities determined at the ITRF co-locations reported in Table 5. Results are plotted per component and per time segment. The same conventions on the *colors* of Fig. 6 have been adopted. In the abscissae, the DOMES numbers of the ITRF co-location sites used for the TCH analyses are reported. *The black solid lines* reported in all of the plots marks the $\rho = 1$ value

again to the presence of technique-dependent biases which are not reflected either in the WRMS or in the formal errors of the SLR stations.

Remarkable discrepancies ($\rho \gg 2$) can be observed in the east and north components at some GPS sites. These are once again indicative of low-quality GPS stations such as METS, AREQ, TIDB (50119, Tidbinbilla, Australia) and STR1 (50103, Mount Stromlo, Australia). It is worth observing that STR1 is the most affected by time-correlated errors in that the amount of flicker noise exceeds the 10 mm/$y^{0.25}$ level in each of the three components.

The plots of Fig. 8 represent the ratio R = TCH/σ between TCH and the median formal errors for each SG techniques at the co-locations of Table 4. R provides an indication of the scaling factor to apply to the station formal errors as reported in the SINEX files in order to obtain a more realistic description of the SG technique uncertainties. Ratios larger (smaller) than 1 indicate the TCH-derived sigmas are higher (lower) than the median formal errors, thus suggesting the uncertainties be up-scaled (down-scaled).

Table 6 reports the median values of the ratios R and compares them with the AVFs derived from the single-technique stacks described in Sect. 3. If on the one hand, VLBI, SLR and DORIS are characterized by median $R > 1$, GPS on the other proves to have median $R < 1$ on all of the three components. GPS is therefore the only SG technique whose covariances are not to be up-scaled. Also, it is worth noticing the height component median ratio R compares rather well with the AVF estimated through the stacking (cf. Table 6).

As to VLBI, the plots of Fig. 8 clearly show there is no overall agreement between the ratios and the AVF. Median R reported in Table 6 prove the VLBI covariances have to be scaled by a factor of $\sim$2, which is lower than what the AVF suggests (5.5).

As to SLR, the height median value of the ratio R suggests the height component of the covariances be up-scaled by a factor 5, whereas the horizontal median ratios are 1.5 and 1.6 for the north and height components, respectively. The AVF derived from the SLR stack does not prove to be in agreement with the ratios in any of the three components (cf. Table 6).

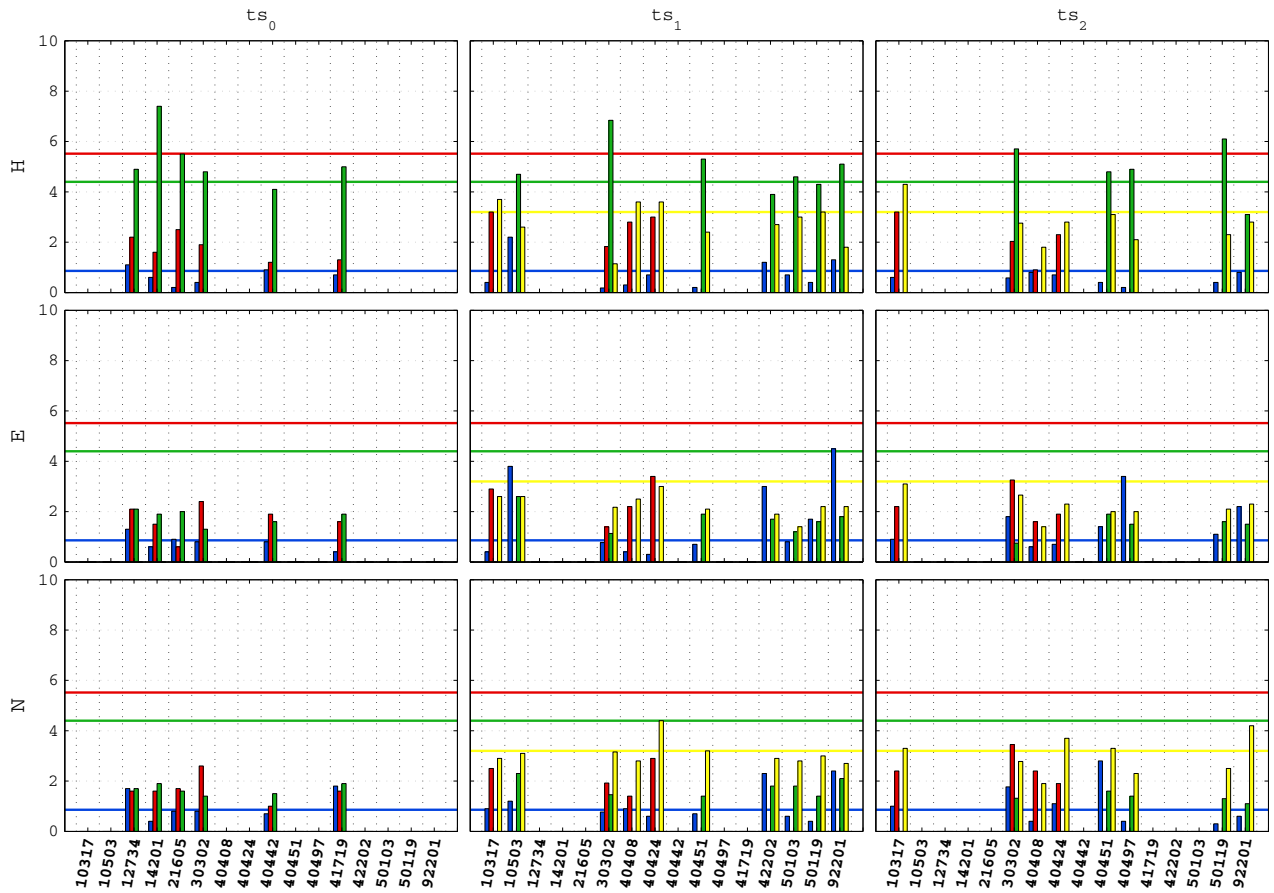

Fig. 8 *Bar plot* of the ratio $R = \mathrm{TCH}/\sigma$ between the TCH-derived sigmas and the median formal errors relevant to the ITRF co-locations reported in Table 5. Values are plotted per component and per time segment (ts_0, ts_1 and ts_2). The same conventions on the *colors* of Fig. 6 have been adopted. *The solid lines* mark the square root of the AVFs derived from the stacks of the 4 SG techniques reported in Table 6. In particular, *the blue solid line* marks the value 0.9 representing the square root of the AVF for GPS: *the red solid line* marks the value 5.5 which is the square root of VLBI AVF; *the green solid line* marks the value 4.4 representing the AVF of SLR, whereas *the yellow solid line* corresponds to the value 3.2 and represents the square root of the AVF for DORIS

The median ratios for DORIS exhibit values of 3.0, 2.2 and 2.8 for the north, east and height component, respectively, and compare well with the corresponding AVF of 3.2 as reported in Table 6.

6 Conclusions

The application of TCH to time series of SG residual positions has been critically discussed and results have been provided analysing the ITRF2008 datasets. The major advantage of adopting TCH lies in the removal of common-mode signals at co-located sites when pair-wise differences are formed. In the absence of specific technique-dependent biases, TCH estimates uniquely reflect the SG measurement errors. Conversely, intrinsic metrics based on post-fit residuals such as RMS, WRMS and AVFs factors are unavoidably affected by the presence of non-linear geophysical signals.

Adopting simulations of stochastic processes, we investigated the impact of different levels of intrinsic precisions of the 4 SG techniques and of time-correlated errors on TCH. We found that, in the absence of time-correlated errors, TCH is able to fully recover the nominal uncertainties of groups of observations whose intrinsic precisions are remarkably dissimilar. When time-correlated errors are largely predominant, TCH is affected by the increased variance of the observations.

To provide TCH estimates free from technique-specific systematic effects, GPS and DORIS draconitic signatures have been removed from the SG residual positions. TCH estimates have been determined for 16 co-located sites provided with a sufficient number of simultaneous observations. Considering the reduced number of 3-way co-locations available, our results cannot be regarded as representative of the entire SG networks. This is particularly true for SLR, where many of the high-quality stations such as Yarragadee (Australia),

Herstmonceux (UK), Graz (Austria) and Grasse (France) could not be included in the analyses.

TCH applied to the selected co-locations confirmed that GPS, albeit affected by time-correlated errors, is the most precise of the SG techniques. GPS TCH median values are 1.1, 1.2 and 2.8 mm, for the north, east and height component, respectively. VLBI performs particularly well in the horizontal components, its median uncertainties being in the order of 2 mm; whereas, its height component is ∼2 times as large as the GPS one. DORIS proved the least precise, their median uncertainties being in the order of 1 cm. The height component uncertainties for SLR and DORIS are three times larger than GPS. None of the 4 SG techniques has proven characterized by sub-millimetric precisions.

We compared TCH determinations with WRMS and found that the two metrics are in striking agreement for VLBI and DORIS but not for GPS and SLR. WRMS can be therefore used as proxy for TCH at the VLBI/DORIS sites wherein the method is not applicable. Co-locations in which TCH estimates are significantly larger than the WRMS are suggestive of site-dependent or technique-dependent biases that neither the formal errors nor the repeatabilities by themselves are able to point out.

Determining the ratio between TCH determinations and median formal errors, we provided a rough estimate of the station-dependent scaling factors to be applied to the covariances of SG solutions in order to get a more realistic description of the uncertainties. Our results suggest the covariances have to be up-scaled for VLBI, SLR, DORIS. The GPS uncertainties of the horizontal components proved in general agreement with the TCH determinations and no scaling would be therefore required. Formal errors of the height component should be down-scaled by a factor 0.6. The TCH-derived scaling factors have also been compared with the AVFs obtained from the stacking of the SG SINEX files. The two metrics compare rather favourably for GPS and DORIS, whereas no agreement has been found for the other SG techniques.

The number of ITRF co-locations which the TCH method may be applied to is still scarce. The larger observing span and the increased amount of SG observations expected for the ITRF2013 might be beneficial thus extending the number of co-locations available for this kind of analyses.

Acknowledgments This research was carried out at the Jet Propulsion Laboratory, California Institute of Technology, under a contract with National Aeronautics and Space Administration. C. Abbondanza wishes to thank J. Ray for the fruitful exchange which contributed to improving the presentation of this manuscript and P. Willis for the useful discussions on the usage of DORIS solutions. D. MacMillan is also gratefully acknowledged for having provided VLBI daily time series adopted to test the Three-Corner Hat at an early stage of this study. We wish to thank J. Ries and three anonymous reviewers for their useful comments and suggestions.

References

Allan DW (1987) Time and frequency (time-domain) characterization, estimation, and prediction of precision clocks and oscillators. IEEE Trans Ultrason Ferroelectr Freq Control UFFC 34(6):647–654. doi:10.1109/T-UFFC.1987.26997

Altamimi Z, Sillard P, Boucher C (2002) ITRF2000: a new release of the International Terrestrial Reference Frame for Earth science applications. J Geophys Res 107(B10):2114–2133

Altamimi Z, Collilieux X, Legrand J, Garayt B, Boucher C (2007) ITRF2005: a new release of the International Terrestrial Reference Frame based on time series of station positions and Earth Orientation Parameters. J Geophys Res 112(B09):401. doi:10.1029/2007JB004949

Altamimi Z, Collilieux X, Métivier L (2011) ITRF2008: an improved solution of the International Terrestrial Reference Frame. J Geod 85(8):457–473. doi:10.1007/s00190-011-0444-4

Amiri-Simkooei AR, Tiberius CCJM, Teunissen PJG (2007) Assessment of noise in GPS coordinate time series: methodology and results. J Geophys Res 112(B7). doi:10.1029/2006JB004913

Beavan J (2005) Noise properties of continuous GPS data from concrete pillar geodetic monuments in New Zealand and comparison with data from US deep drilled braced monuments. J Geophys Res 110(B08):410. doi:10.1029/2005JB003642

Bizouard C, Gambis D (2011) The combined solution C04 for Earth Orientation Parameters consistent with ITRF2008. Technical report, Observatoire de Paris, SYRTE, 61 Av de l'Observatoire, Paris, France. http://hpiers.obspm.fr/iers/eop/eopc04/C04.guide

Böckmann S, Artz T, Nothnagel A (2010) VLBI terrestrial reference frame contributions to ITRF2008. J Geod 84(3):201–219. doi:10.1007/s00190-009-0357-7

Chin TM, Gross RS, Dickey JO (2005) Multi-reference evaluation of uncertainty in Earth Orientation Parameter measurements. J Geod 79(1–3):24–32. doi:10.1007/s00190-005-0439-0

Collilieux X, Altamimi Z, Coulot D, Ray J, Sillard P (2007) Comparison of very long baseline interferometry, GPS and satellite laser ranging height residuals from ITRF2005 using spectral and correlation methods. J Geophys Res 112(B12):403. doi:10.1029/2007JB004933

Collilieux X, Altamimi Z, Ray J, van Dam T, Wu X (2009) Effect of the satellite laser ranging network distribution on geocenter motion estimation. J Geophys Res 114(B04):402. doi:10.1029/2008JB005727

Collilieux X, Métivier L, Altamimi Z, van Dam T, Ray J (2011) Quality assessment of GPS reprocessed terrestrial reference frame. GPS Solut 15(3):219–231. doi:10.1007/s10291-010-0184-6

Collilieux X, van Dam T, Ray J, Coulot D, Métivier L, Altamimi Z (2012) Strategies to mitigate aliasing of loading signals while estimating GPS frame parameters. J Geod 86(1):1–14. doi:10.1007/s00190-011-0487-6

Davis JL, Wernicke BP, Tamisiea ME (2012) On seasonal signals in geodetic time series. J Geophys Res 117(B01):403. doi:10.1029/2011JB008690

Feissel-Vernier M, de Viron O, Le Bail K (2007) Stability of VLBI, SLR, DORIS, and GPS positioning. Earth Planets Space 59(6):475–497

Gambis D (2002) Allan variance in Earth rotation time series. In: Drewes H, Dow JM (eds) New trends in space geodesy, advances in space research, vol 30, pp 207–212. doi:10.1016/S0273-1177(02)00286-7

Gambis D (2004) Monitoring Earth orientation using space-geodetic techniques: state-of-the-art and prospective. J Geod 78(4–5):295–303. doi:10.1007/s00190-004-0394-1

Gobinddass ML, Willis P, de Viron O, Sibthorpe A, Zelensky NP, Ries JC, Ferland R, Bar-Sever Y, Diament M (2009) Systematic biases in DORIS-derived geocenter time series related to solar radia-

tion pressure mis-modeling. J Geod 83(9):849–858. doi:10.1007/s00190-009-0303-8

Hosking JRM (1981) Fractional differencing. Biometrika 68(1):165–176. doi:10.1093/biomet/68.1.165

Kasdin NJ (1995) Discrete simulation of colored noise and stochastic processes and $1/f^{\alpha}$ power law noise generation. Proc IEEE 83(5):802–827. doi:10.1109/5.381848

Koot L, de Viron O, Dehant V (2006) Atmospheric angular momentum time-series: characterization of their internal noise and creation of a combined series. J Geod 79(12):663–674. doi:10.1007/s00190-005-0019-3

Langbein J, Johnson H (1997) Correlated errors in geodetic time series: implications for time-dependent deformation. J Geophys Res 102(B1):591–603

Le Bail K (2006) Estimating the noise in space-geodetic positioning: the case of DORIS. J Geod 80(8–11):541–565. doi:10.1007/s00190-006-0088-y

Mao A, Harrison CGA, Dixon TH (1999) Noise in GPS coordinate time series. J Geophys Res 104(B2):2797–2816. doi:10.1029/1998JB900033

Pavlis E, Luceri V, Sciarretta C, Kelm R (2011) The ILRS contribution to ITRF2008. Technical report. Int Laser Rang Serv, Greenbelt, MD. http://itrf.ensg.ign.fr/ITRF_solutions/2008/doc/ILRSSubmission4ITRF2008. On-line Accessed 1 Sept 2014

Ray J, Altamimi Z, Collilieux X, van Dam T (2008) Anomalous harmonics in the spectra of GPS position estimates. GPS Solut 12(1):55–64. doi:10.1007/s10291-007-0067-7

Ray J, Griffiths J, Collilieux X, Rebischung P (2013) Subseasonal GNSS positioning errors. Geophys Res Lett 40(22):5854–5860. doi:10.1002/2013GL058160

Santamaría-Gómez A, Bouin MN, Collilieux X, Wöppelmann G (2011) Correlated errors in GPS position time series: implications for velocity estimates. J Geophys Res 116(B01):405. doi:10.1029/2010JB007701

Sillard P, Boucher C (2001) A review of algebraic constraints in terrestrial reference frame datum definition. J Geod 75:63–73. doi:10.1007/s001900100166

Tregoning P, van Dam T (2005) Effects of atmospheric pressure loading and seven-parameter transformations on estimates of geocenter motion and station heights from space geodetic observations. J Geophys Res 110(B3). doi:10.1029/2004JB003334

Valette JJ, Lemoine FG, Ferrage P, Yaya P, Altamimi Z, Willis P, Soudarin L (2010) IDS contribution to ITRF2008. Adv Space Res 46(12):1614–1632. doi:10.1016/j.asr.2010.05.029

Williams SDP (2003) The effect of coloured noise on the uncertainties of rates estimated from geodetic time series. J Geod 76(9–10):483–494. doi:10.1007/s00190-002-0283-4

Williams SDP (2008) CATS: GPS coordinate time series analysis software. GPS Solut 12(2):147–153. doi:10.1007/s10291-007-0086-4

Williams SDP, Bock Y, Fang P, Jamason P, Nikolaidis RM, Prawirodirdjo L, Miller M, Johnson DJ (2004) Error analysis of continuous GPS position time series. J Geophys Res 109(B03):412. doi:10.1029/2003JB002471

Wyatt F (1982) Displacement of surface monuments: horizontal motion. J Geophys Res 87(B2):979–989

Wyatt F (1989) Displacement of surface monuments: vertical motion. J Geophys Res 94(B2):1655–1664

Zhang J, Bock Y, Johnson H, Fang P, Williams S, Genrich S, Wdowinski S, Behr J (1997) Southern California permanent GPS geodetic array: error analysis of daily position estimates and site velocities. J Geophys Res 102(B08):18035–18055. doi:10.1029/97JB01380